X-Ray Structure Determination of Fully Hydrated L_α Phase Dipalmitoylphosphatidylcholine Bilayers

John F. Nagle,*‡ Ruitian Zhang,* Stephanie Tristram-Nagle,‡ Wenjun Sun,* Horia I. Petrache,* and Robert M. Suter*
*Department of Physics and ‡Department of Biological Sciences, Carnegie Mellon University, Pittsburgh, Pennsylvania 15213

ABSTRACT Bilayer form factors obtained from x-ray scattering data taken with high instrumental resolution are reported for multilamellar vesicles of L_α phase lipid bilayers of dipalmitoylphosphatidylcholine at 50°C under varying osmotic pressure. Artifacts in the magnitudes of the form factors due to liquid crystalline fluctuations have been eliminated by using modified Caillé theory. The Caillé fluctuation parameter η_1 increases systematically with increasing lamellar D spacing and this explains why some higher order peaks are unobservable for the larger D spacings. The corrected form factors fall on one smooth continuous transform $F(q)$; this shows that the bilayer does not change shape as D decreases from 67.2 Å (fully hydrated) to 53.9 Å. The distance between headgroup peaks is obtained from Fourier reconstruction of samples with four orders of diffraction and from electron density models that use 38 independent form factors. By combining these results with previous gel phase results, area A^F per lipid molecule and other structural quantities are obtained for the fluid L_α phase. Comparison with results that we derived from previous neutron diffraction data is excellent, and we conclude from diffraction studies that $A^F = 62.9 \pm 1.3$ Å^2, which is in excellent agreement with a previous estimate from NMR data.

INTRODUCTION

Obtaining the average bilayer structure of the benchmark lipid, dipalmitoylphosphatidylcholine (DPPC), in the biologically relevant, fully hydrated, L_α phase has been very challenging. Estimates for area A per molecule span an unacceptably large range (Nagle, 1993) from 58 Å^2 to 71 Å^2, and there are corresponding uncertainties in bilayer thickness. These uncertainties have inhibited the understanding of the biophysical differences between bilayers composed of different lipids. Reducing this uncertainty and obtaining additional structural data for DPPC will provide more stringent tests of the potentials employed in molecular dynamics simulations of membranes.

One of the major problems in determining the structure of DPPC bilayers in the L_α (synonymously the fluid, chain-melted, or liquid-crystalline) lamellar phase is the small number of observable orders of diffraction when the sample is fully hydrated. More orders of diffraction can be observed at reduced hydration levels, but the most direct explanation for this is that the bilayer structure changes with hydration. If this explanation were correct, then the strategy of reducing the hydration level to obtain bilayer structure would seem to be biologically equivocal, because biological membranes are usually fully hydrated.

On the other hand, the loss of higher orders of diffraction with increasing hydration could be due to increased undulation fluctuations, which also systematically reduce the size of the higher order peaks that one can measure. The theory for this has been carefully developed (Zhang et al., 1994), and we have obtained synchrotron data at high instrumental resolution that verify that the peak shapes are well described by the theory (Zhang et al., 1995, 1996). One of the main results of this paper is the presentation of the corrected form factors for many different lamellar D spacings. These form factors fit well on a single continuous transform $F(q)$ as is required if the bilayers do not change structure upon dehydration. This suggests that some very careful previous studies on partially dehydrated samples (e.g., Buldt et al., 1979; Wiener and White, 1992) may be appropriate for the biologically relevant fully hydrated L_α phase.

A standard way to analyze low angle x-ray structural data is to plot the Fourier reconstruction from the form factors for the observable peaks (McIntosh and Simon, 1986a,b). A primary result from such plots is the head-head spacing X_{HH}. Our theory (Zhang et al., 1994) shows that X_{HH} changes very little when corrections due to fluctuations are made and this will be illustrated with the present data. The largest change due to fluctuation corrections is to sharpen the features in the electron density profiles.

The preceding improvements culminate in electron density profiles that should be useful when compared to molecular dynamics simulations and that give a measure of the head-head spacing X_{HH}. Although the latter is often interpreted as the phosphate-phosphate distance, this may not be literally true; and it is certainly not possible to obtain hydrocarbon thicknesses nor interfacial areas A from electron density profiles, even in the gel phase (Wiener et al., 1989). In the case of the gel phase, one has additional information from the sharp wide angle peaks, such as chain area A_c and tilt angle θ (Tristram-Nagle et al., 1993; Sun et al., 1994) that enable a fairly complete average structure determination. For dilaurylphosphatidyletha-

Received for publication 2 October 1995 and in final form 15 December 1995.

Address reprint requests to Prof. J. F. Nagle, Department of Physics, Carnegie Mellon University, Pittsburgh, PA 15213. Tel.: 412-268-2768; Fax: 412-681-0648; E-mail:jn12+@andrew.cmu.edu.

0006-3495/96/03/1419/13 $2.00

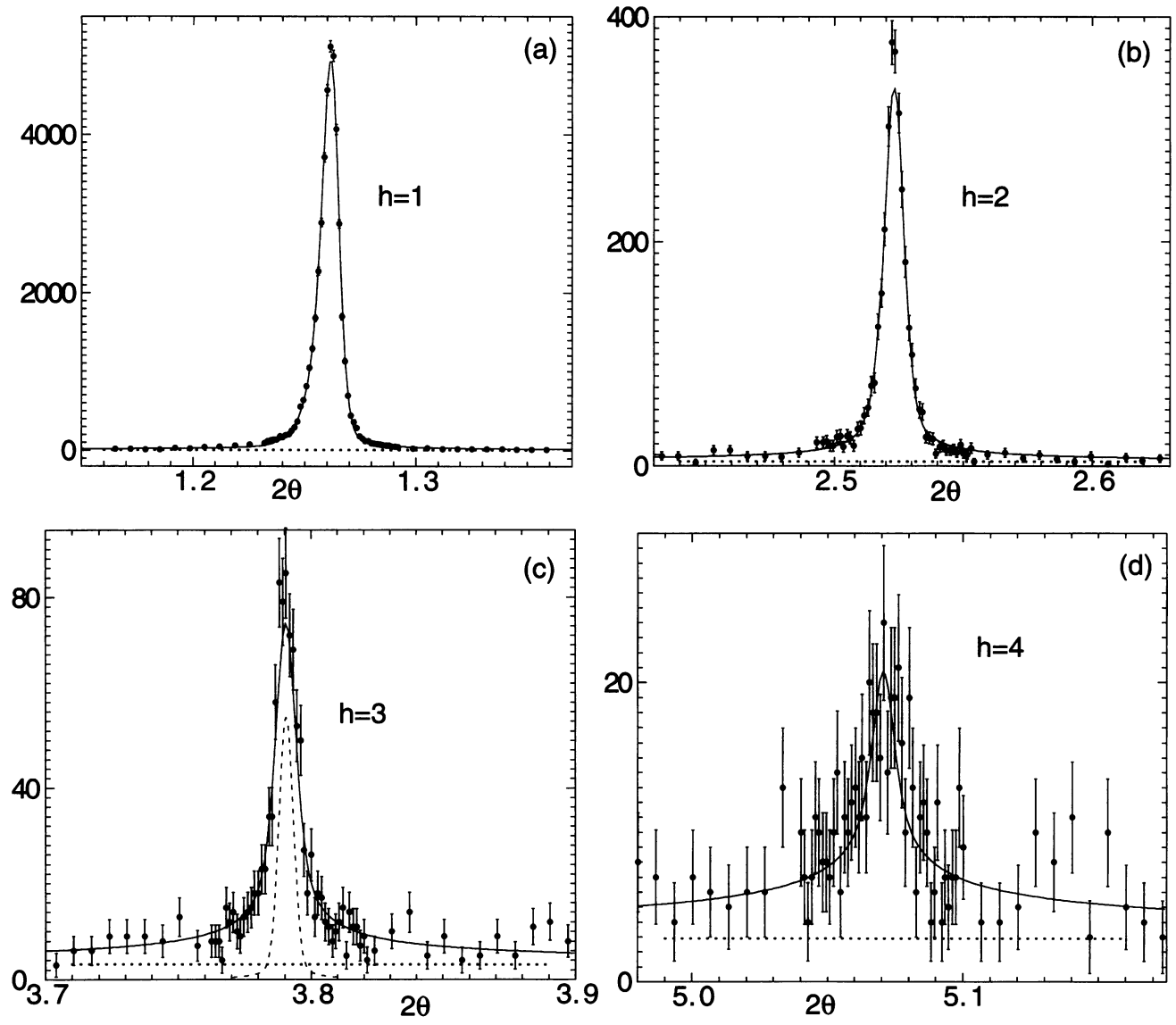

FIGURE 1 Counts versus scattering angle 2θ (degrees) for the first four orders from a sample of DPPC with D = 55.06 Å. The solid lines show simultaneous fits to all orders using Eq. 2 with reduced χ^2 = 1.8. The dashed curve in (*c*) shows the longitudinal resolution. The horizontal dotted lines show the background levels whose estimated uncertainties are roughly 10%.

nolamine (DLPE) bilayers, McIntosh and Simon (1986b) showed how to obtain the structure of the L_α phase, especially the evasive area of the fluid phase A^F, by using gel phase structure together with measured differences between the gel and fluid phases in headgroup spacing X_{HH} and lipid volumes. Essentially the same procedure is applied in this paper for the structure of the L_α phase of DPPC.

EXPERIMENTAL

Full experimental details for obtaining the data in this paper have recently been presented (Zhang et al., 1996). Briefly, DPPC (1,2-dipalmitoyl-*sn*-glycero-3-phosphatidylcholine) from Avanti Polar Lipids (Alabaster, AL) was dispersed in pure water or aqueous polyvinylpyrrolidone (PVP) solutions and sealed in thin walled glass capillaries. The maximum PVP concentration was nominally 50% (w/w), which corresponds to 98% relative humidity (McIntosh and Simon, 1986a). All data were taken from samples at 50°C.

High resolution x-ray scattering experiments were performed at the Cornell High Energy Synchrotron Source (CHESS) on the F3 station. A double bounce Si monochromator was calibrated to 1.2147 Å x rays, the scattering angles were selected by Bragg diffraction from the (111) face of a Si analyzer crystal, and the intensity was measured by a NaI scintillation detector. The longitudinal resolution had half width at half maximum of either 1.0×10^{-4} Å^{-1} or 3.3×10^{-4} Å^{-1}. The out-of-scattering plane resolution was 6×10^{-3} Å^{-1} and this caused a small amount of slit smearing in the first order peak that was, however, easily accommodated in the theoretical fits to the data.

Significant radiation damage, as detected by observing changes in peak shapes and positions and by thin layer chromatography, was avoided by systematically exposing different spots on the capillary of the same sample to the x-ray beam (Zhang et al., 1996). To obtain the relative intensities of different orders measured on different spots, brief scans of the intense first order peak were taken on each spot for normalization. Weak background

scattering from capillaries containing air, pure water, 25% PVP solution, and 50% PVP solution was measured using long counting times. The angular range of the reported data for the tails of the peaks was restricted so that the average intensity was at least twice as great as the background. Typical data are shown in Fig. 1.

THEORY

A scattering theory that allows for bending of the bilayers in addition to fluctuations in the mean spacings between bilayers and that is based on energetics of both kinds of fluctuations was originally presented by Caillé (1972), who built upon the thermodynamic theory of smectic liquid crystals summarized by DeGennes (1974). This is a rather deep physical theory that gives rise to non-Bragg scattering peaks with long power law tails that conceal much of the true scattering intensity and thereby artifactually reduce the apparent form factor monotonically as a function of the order h of the peak. In the Caillé theory the primary fluctuation parameter is

$$\eta = \frac{q^2 kT}{8\pi\sqrt{KB}}, \tag{1}$$

which involves the bending modulus K of lipid bilayers and the bulk modulus B for compression; the wave vector q has the value $2\pi h/D$ at the h-th order peak and kT is the thermal energy. Because each peak is sharp and well separated from other peaks, it is customary to report just η_1, which is defined to be the value of η at q_1 for the $h = 1$ first order peak, recognizing that η near the h-th order peak is given by

$$\eta_h = \eta_1 h^2. \tag{2}$$

Because the size of the peak tails relative to the central peak grows with the size of η, higher order peaks are more affected by fluctuation artifacts than lower order peaks.

We have modified the Caillé theory in a recent theoretical paper (Zhang et al., 1994). Our modifications did not affect any of the qualitative results in this theory, but they were necessary for obtaining better quantitative fits to powder data, and particularly for extracting the correct form factors to be used for obtaining electron density profiles. Detailed fits to some of our data were shown in previous papers (Zhang et al., 1995, 1996). The primary parameters in these fits are η_1, the mean size of domains L, and the root mean square distribution σ_L of domain size as described in detail by Zhang et al. (1994, 1996).

RESULTS

Basic data: form factors and fluctuation parameters

Fig. 1 shows data for one sample in 40% PVP aqueous solution and the fits from the theory. By varying the concentration of PVP in aqueous solution containing the multilamellar vesicles of DPPC, we have obtained D spacings that range from 67.2 Å with pure water to 53.9 Å with 50% PVP in a total of 21 samples.

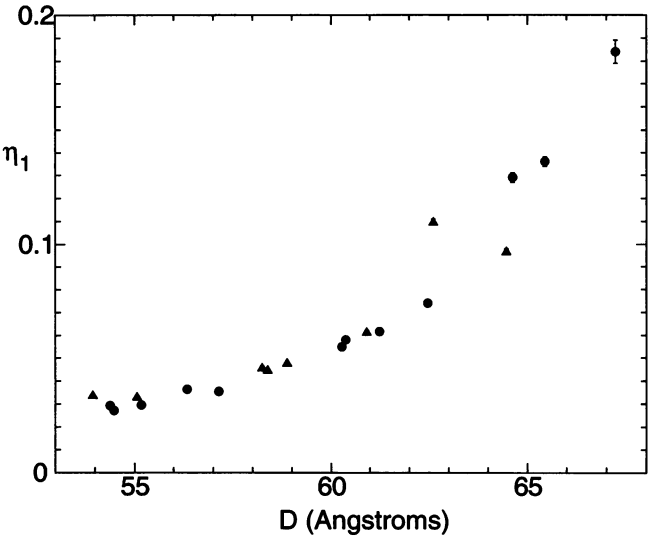

FIGURE 2 Caillé fluctuation parameter η_1 for 21 samples versus the D spacing. Solid circles indicate highest resolution (0.0001 Å^{-1}) data and solid triangles indicate lower resolution (0.0003 Å^{-1}) data taken on different synchrotron runs. All observed peaks were fit simultaneously.

A detailed simultaneous fit to all the observed peaks of each sample, as illustrated in Fig. 1, yields the fluctuation parameter η_1 for each sample; η_1 is plotted versus D in Fig. 2. Fig. 2 shows a systematic decrease in the fluctuation parameter η_1 with decreasing D (decreasing hydration). Because the higher order scattering peaks become unobservable when η_h becomes large (somewhat in excess of unity; see Fig. 2 in Zhang et al. (1996)) and because η_h grows with h according to Eq. 2, Fig. 2 gives one reason why there are fewer observable peaks for more hydrated samples than for less hydrated samples.

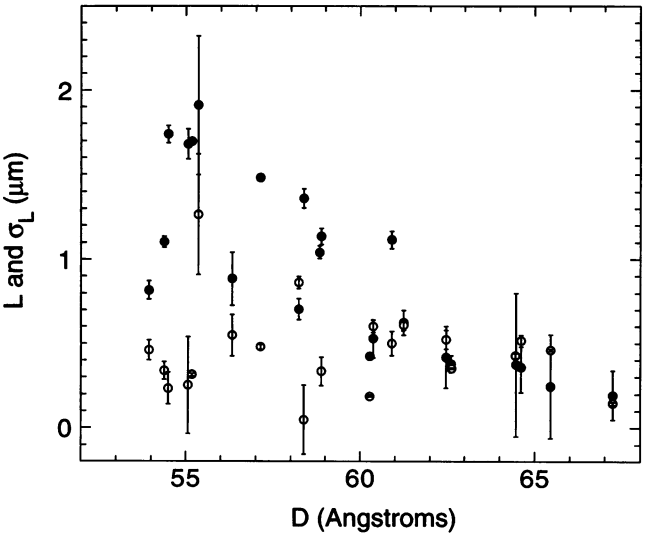

FIGURE 3 The mean length of scattering domains L (*solid circles*) along the bilayer normal and the mean dispersion σ_L in L (*open circles*) versus D spacing.

Other parameters in fitting the scattering peak shapes are the mean domain size L and the dispersion σ_L in the distribution of domain sizes (Zhang et al., 1996). Results for these parameters versus D are shown in Fig. 3. There is some trend toward greater domain sizes L with decreasing D, but it is far less systematic than the dependence of η_1 on D in Fig. 2. This can be attributable to extraneous factors in sample preparation, such as the extent of annealing that affects the sizes of the multilamellar vesicles. Indeed, L is not a fundamental parameter that reports interactions between bilayers. The fact that the results in Fig. 2 are quite smooth compared to those in Fig. 3 is evidence that there is little correlation between the values of η_1 and L and that the values of η_1 in Fig. 2 are not artifacts of sample preparation.

Our fits to the data and the values of η_1 allow the long tails of the peaks to be extrapolated and the total intensity under the hth order peaks to be recovered. Then, using the standard formula (Zhang et al., 1994),

$$I_h = |F_h|^2/q_h^2, \quad (3)$$

the absolute values of the form factors $F_h = F(q_h)$ were obtained. The phases $(-, -, +, -)$ of these form factors are well known from other studies (McIntosh and Simon, 1986a) and will be confirmed later by our studies of electron density profiles. The form factor data are presented in Table 1. There is no reliable way to measure the relative magnitude of form factors with different concentrations of PVP and different D spacings because they involve different samples. When a large number of orders are measured, one can use the standard method based on Parseval's theorem (Worthington, 1969) to normalize the form factors independently for each sample. We used this to obtain a first normalization, but this is not accurate enough when so few orders are available and when higher orders are suppressed by undulation fluctuations. Therefore, the primary data are presented in Table 1 as ratios $f_h = F_h/F_1$ of the higher order form factors F_h to the first order form factor F_1 for each of the 21 samples. Table 1 also shows the correction factor R_{max} for the highest order observable peak for each sample. The correction factor is the ratio of the uncorrected form factor to the corrected form factor. The uncorrected form factor was obtained by simple integration of the background subtracted peak to the end of the data range where the background became comparable to the signal. In the final column in Table 1 are shown the values of F_1, obtained after fitting all the form factors to a model as will be discussed below. To obtain our best estimate of the form factors F_h for $h > 1$, multiply each f_h by F_1. However, it should be emphasized that the basic data are only the ratios represented by the f_h, of which there are 38 independent values in Table 1.

TABLE 1 Form factors of L_α phase dipalmitoylphosphatidylcholine bilayers

D (Å)	f_2	f_3	f_4	R_{max}	F_1 (1G fit)
67.23	1.41 (0.09)	0.0 (0.1)*	0.0 (0.2)*	0.75	1.49
65.45	1.26 (0.04)	0.0 (0.1)*	0.0 (0.2)*	0.79	1.53
64.62	1.23 (0.05)	0.0 (0.1)*	0.0 (0.2)*	0.79	1.56
64.47	1.32 (0.03)	0.00 (0.08)*	0.0 (0.1)*	0.79	1.56
62.61	1.27 (0.03)	0.0 (0.1)*	0.0 (0.2)*	0.79	1.63
62.46	1.14 (0.03)	0.0 (0.1)*	0.0 (0.2)*	0.82	1.63
61.24	1.10 (0.02)	0.52 (0.03)	0.0 (0.1)*	0.71	1.66
60.91	1.09 (0.03)	0.57 (0.05)	0.00 (0.09)*	0.72	1.67
60.37	1.02 (0.02)	0.55 (0.03)	0.0 (0.2)*	0.69	1.70
58.88	0.89 (0.02)	0.57 (0.03)	—	0.77	1.76
58.84	0.86 (0.03)	0.60 (0.05)	—	0.77	1.76
58.38	0.89 (0.02)	0.65 (0.03)	0.61 (0.06)	0.82	1.77
58.24	0.90 (0.02)	0.67 (0.04)	—	0.79	1.78
57.14	0.75 (0.01)	0.50 (0.03)	—	0.88	1.82
56.33	0.71 (0.03)	0.57 (0.04)	—	0.68‡	1.85
55.35	0.65 (0.02)	0.54 (0.04)	—	0.89	1.88
55.18	0.58 (0.02)	0.48 (0.03)	—	0.88	1.89
55.06	0.60 (0.02)	0.59 (0.03)	0.65 (0.05)	0.75	1.89
54.49	0.55 (0.02)	0.40 (0.04)	0.43 (0.07)	0.49‡	1.92
54.38	0.49 (0.06)	—	—	0.88§	1.92
53.94	0.536 (0.008)	0.57 (0.03)	—	0.81	1.94

Estimated errors are shown in parentheses, $f_h = F_h/F_1$ and $R_{max} = f^{unc}_{h_{max}}/f_{h_{max}}$

*Indicates peak whose uncorrected intensity is below our detection limit. For uncorrected f_h^{unc}, integration limits are $\Delta 2\theta = 0.2°$, except: ‡: $\Delta 2\theta = 0.06°$, and §: $\Delta 2\theta = 0.04°$.

Continuous transforms and test of dehydration threshold hypothesis

The first major issue to test with the data in Table 1 is whether 1) partial dehydration changes the structure of the bilayer, such as the thickness, or whether 2) partial dehydration consists simply of taking water out of the space between bilayers leaving the bilayers essentially unchanged. It is unlikely that bilayer structure will remain unchanged for strong dehydration that removes nearly all the water, so it is important to emphasize that the word partial in the

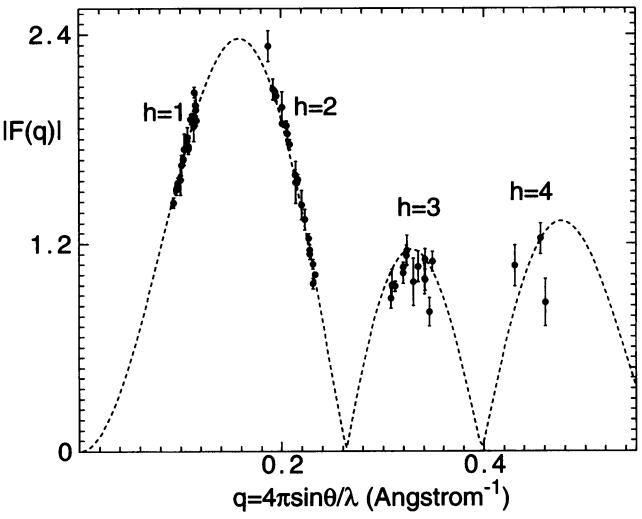

FIGURE 4 The dashed curve shows the continuous transform obtained from the four orders of the $D = 55.06$ Å sample. The solid circles show the corrected form factors for all 21 samples, each set of form factors for each sample was scaled simultaneously for all orders to give the best fit to the dashed curve. $F(0)$ is set to zero from volume measurements.

statement of the hypothesis 2 means that there is a threshold spacing D_T smaller than the fully hydrated spacing D_{FH} such that for D spacing between D_T and D_{FH} there is no effective change in bilayer structure. We will refer to hypothesis (2) as the threshold hypothesis. Although it is likely that there will be an effect on the bilayer structure caused by any change in interlamellar forces that must accompany any level of dehydration, the effect would be expected to be negligible for mild dehydration if the interlamellar interactions are weak compared to the intralamellar interactions when the water spacing is large enough (Nagle, 1980).

The standard way to test the dehydration hypothesis is to observe whether the form factors for all the samples fall on a single continuous transform $F(q)$ (Torbet and Wilkins, 1976; McIntosh and Simon, 1986a). In this subsection this is accomplished first by obtaining a trial $F(q)$ using the sampling theorem (Worthington et al., 1973) and four measured orders of diffraction from one of the more dehydrated samples. A scale factor is then chosen for each remaining sample to minimize the weighted differences of the discrete form factors with the trial $F(q)$. The result of this procedure, shown in Fig. 4, indicates that the fluctuation-corrected form factors belong to a single continuous transform, thereby supporting the threshold hypothesis and negligible change in bilayer structure over the range of dehydration of our data.

Fig. 4 is drawn with $F(0) = 0$. This value follows from the general relation (Nagle and Wiener, 1989),

$$F(0) = 2(n_L^* - V_L\rho_W^*)/A. \quad (4)$$

Using the number of electrons $n_L^* = 406$ in a DPPC molecule, the measured volume of DPPC molecules $V_L = 1232$ Å^3 at 50°C (Nagle and Wiener, 1988) and the density of electrons in water $\rho_W^* = 0.330$ Å^{-3} at 50°C gives a nearly zero numerator on the right hand side of Eq. 4 so that for any reasonable estimate of A one has $F(0) \sim -0.02e/$Å^2. The value of $F(0)$ is $1.0e/$Å^2 for the gel phase (Wiener et al., 1989) and the absolute values of F_1 (to be obtained later) exceed $2e/$Å^2. Compared with these, $F(0)$ for the fluid phase is negligible and will be taken to be zero in this paper.

It is important to examine why our corrections to the form factors are essential. Fig. 5 shows a continuous $F(q)$ curve obtained from uncorrected form factors in the same way as the $F(q)$ curve in Fig. 4 was obtained from the corrected form factors. In Fig. 5 all the first order form factors have been placed on the $F(q)$ curve. Then, it is seen that the second order form factors also fall on the $F(q)$ curve for small D, but that for $D > 61$ Å ($q_2 < 0.205$ Å^{-1}) the second order form factors systematically fall below the $F(q)$ curve. If one had no reason to correct these form factors, one would have to draw the conclusion that the bilayer structure changes as full hydration is approached. However, this conclusion is not warranted, because these are the form factors that require the largest corrections because η_1 is greatest for these samples. As is shown in Fig. 4 the corrections bring these form factors back onto the $F(q)$ curve.

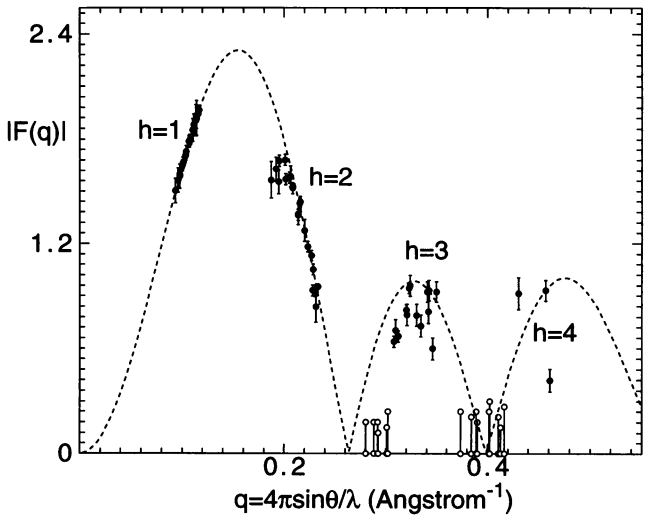

FIGURE 5 The dashed curve shows the continuous transform obtained from the uncorrected four orders of the $D = 55.06$ Å sample. The solid circles show the form factors for all 21 samples with each $F(1)$ placed on the $F(q)$ curve. Open circles indicate peaks not seen whose uncorrected form factors are estimated to be bounded by the pair of circles joined by a vertical line.

A similar, but less dramatic, trend occurs for the $h = 3$ form factors with the largest D spacings. In Fig. 5 estimated ranges (as indicated in Table 1 by * entries) are shown for peaks that we attempted to observe but could not because they were too weak; the largest value for these ranges indicates our estimate of the smallest peak that we could have seen with our apparatus. The unobservability of the $h = 4$ peaks is not

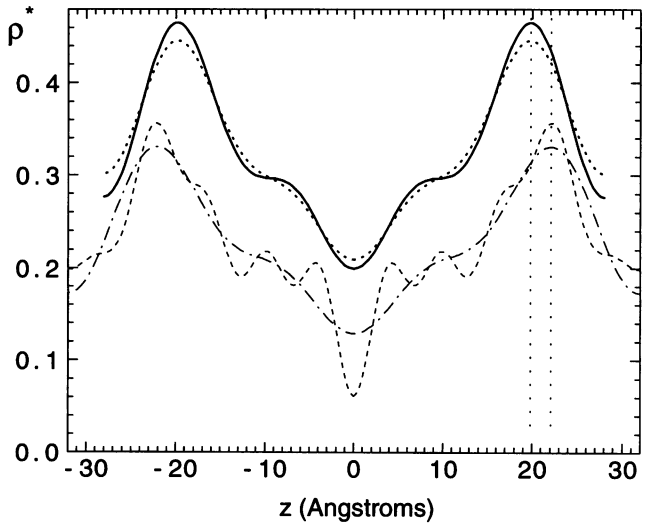

FIGURE 6 Electron density profiles $\rho^*(z)$, in absolute units of electrons/Å^3, as a function of z along the bilayer normal with the center of the bilayer at $z = 0$, obtained by Fourier reconstruction with phases (−, −, +, −). *Solid line*: average from three samples of L_α phase DPPC using four orders of diffraction. *Dotted line*: same average except that uncorrected form factors were used. *Dash-dot line*: gel phase DPPC using four orders, from Wiener et al. (1989). *Dashed line*: gel phase DPPC using ten orders. To avoid overlapping, the gel phase curves have been displaced downwards by −0.1 electrons/Å^3. Also, ρ_W^* has been added.

surprising because most of them have q values that fall near a zero in the $F(q)$ transform. However, some of the unobserved $h = 3$ peaks would, without our correction theory, not follow the $F(q)$ curve and would therefore also lead to the erroneous conclusion that the bilayer structure changes as full hydration is approached. Because the correction for these unobserved peaks is even larger than R_{max}^{-1} shown in Table 1, the corrected ranges are larger than shown in Fig. 5 and overlap the continuous transform in Fig. 4.

Fourier reconstruction of electon density profiles

Electron density $\rho^*(z)$ profiles are easily obtained by Fourier reconstruction from the measured form factors. This method by itself can only give relative electron densities because there is an arbitrary scale factor for each sample. However, our modeling studies to be described later give estimates for these scale factors; these are used in the Fourier electron density profiles in Fig. 6, which are therefore displayed in absolute units. There are three different samples for which we obtained fourth order form factors and we have averaged these electron density profiles using the standard phases $(-, -, +, -)$. The resulting solid curve in Fig. 6 shows a terminal methyl trough centered at the middle of the bilayer at $z = 0$ and two headgroup peaks, with head-head separation $X_{HH} = 39.6$ Å. For comparison, the electron density profile obtained from the uncorrected form factors is shown by a dotted curve in Fig. 6. This latter profile has (1) wider headgroup peaks and methyl trough, but (2) the position of the headgroup peak is very close to the position of the headgroup peak in the fluctuation corrected profile shown by the solid curve in Fig. 6. Both these properties follow from the general theory (Zhang et al., 1994). These results were also anticipated in earlier studies that postulated phenomenological Debye-Waller factors (Franks and Lieb, 1979; Torbet and Wilkins, 1976; Zaccai et al., 1975). Some details of our derivation and differences with the preceding ideas are given in the Appendix. The significance of this result for evaluation of earlier fluctuation uncorrected analyses of bilayer structure is that estimates of head-head spacing X_{HH} should be reliable, but widths of structural features such as headgroups will have been overestimated. Fortunately, X_{HH} has been the important quantity for most applications (McIntosh and Simon, 1986a,b).

Fig. 6 also shows the Fourier reconstructions of the DPPC gel phase electron density profile with 4 orders and with 10 orders (Torbet and Wilkins, 1976). It is remarkable that X_{HH} is essentially the same for both these reconstructions, especially because it is smaller by 2 Å for $h_{max} = 6$ and by 1 Å for $h_{max} = 8$ (Wiener et al., 1989). There is also evidence that this fortuitous accuracy in the $h = 4$ value for X_{HH} appears to hold for the fluid phase as well. This evidence comes from Fourier analyzing the electron density profile obtained from molecular dynamics simulations (Tu et al., 1995) and reconstructing the Fouriers for various orders h. The peak position of the electron density from the simulation is at $z = 18.3$ Å and the peak positions for the Fouriers are 18.9 Å ($h = 2$), 19.9 Å ($h = 3$), 18.3 Å ($h = 4$), 19.2 Å ($h = 5$) and 18.6 Å ($h = 6$). The difference in X_{HH} from the gel phase to the fluid phase will be important in the next subsection; half this difference ΔX_H is indicated by the distance between the vertical dashed lines in Fig. 6.

Method for determining A from X_{HH}

One of our main goals has been to obtain the area A per lipid molecule at the water/bilayer interface. Because this involves information about the structure in the direction along the surface of the bilayer, whereas low angle scattering involves information along the direction of the bilayer normal, other information must be used. We will adapt a method introduced by McIntosh and Simon (1986b) and applied by them to DLPE. This method makes use of the well-determined gel phase quantities and of measured differences with the L_α phase. The quantities involved are area A, lipid volume V_L, hydrocarbon chain thickness D_C, which is half the thickness of the hydrocarbon region in a bilayer, and head-head spacing X_{HH}; superscript G will designate gel phase and superscript F will designate fluid (L_α) phase quantities. The method begins with the statement that the change in volume takes place only in the hydrocarbon region, so

$$V_L^F - V_L^G = A^F D_C^F - A^G D_C^G \tag{5}$$

The justification for assuming that there is little change in volume of the headgroup region is that water can freely enter this region and fill any volume that is voided by the headgroups in going from the gel to the fluid phase (see Wiener et al. (1988) or Nagle and Wilkinson (1978) for more discussion of this assumption). We next write

$$D_C^F = D_C^G + [X_{HH}^F - X_{HH}^G]/2, \tag{6}$$

which assumes that the major determinant of changes in X_{HH} is changes in the hydrocarbon region. Even though the headgroups might be expected to adopt a different mixture of conformations in the two phases, the lever arm for distance changes due to headgroup changes is short, essentially from the carbonyls to the phosphate because the choline is not electron dense, so that Eq. 6 should be a reasonable first approximation. It may be noted, however, that the assumptions behind both Eq. 5 and Eq. 6 should be subject to testing and possible modification by molecular dynamics simulations. Solving Eqs. 5 and 6 yields

$$A^F = [V_L^F - V_L^G + A^G D_C^G]/[D_C^G - (X_{HH}^G - X_{HH}^F)/2]. \tag{7}$$

To apply Eq. 7 we use volume measurements summarized by Nagle and Wiener (1988) that gave $V_L^F = 1232$ Å^3 at 50°C and $V_L^G = 1144$ Å^3 at 20°C. Our best wide angle x-ray determination of the gel phase (Sun et al., 1994) gives $A^G = 47.9$ Å^2 and $D_C^G = 17.23$ Å (corrected from 24°C to 20°C). Using the values $X_{HH}^G = 44.2$ Å and $X_{HH}^F = 39.6$ Å

obtained from Fig. 6 and the preceding subsection, Eq. 7 then gives $A^F = 61.2$ Å^2.

Hybrid models

Fourier reconstruction of electron density profiles has some disadvantages; 1) it is intrinsically on a relative scale rather than an absolute scale, 2) it can only use form factors from one sample at a time, and 3) it has obviously unreal Fourier wiggles. An alternative is to specify a reasonable functional form for the electron density that involves several parameters that are then fit to provide the best agreement with the measured intensities. (Notice that the phases of the form factors are output, not input.) The particular electron density model that will be employed in this subsection is called the one Gaussian (1G) hybrid model (Nagle and Wiener, 1989). This model has one Gaussian representing each headgroup with three parameters (position, width, and height), a Gaussian methyl trough with two parameters (width and depth with position fixed at zero), a known constant water electron density and a constant methylene electron density $\rho^*_{CH_2}$. If one of the electron density amplitude parameters can be predetermined, then hybrid model electron densities can be put on an absolute scale. Furthermore, all the form factors for all the data from different samples at different D spacings can be used on an equal footing to determine the best values of the parameters in the model. We have measured 59 form factors, many more than the 21 scaling factors plus the number of unknown parameters (six for the 1G hybrid model described above and nine if two Gaussians represent each headgroup as in a 2G hybrid model). If there were no experimental error in the form factors, these data would allow determination of quite realistic electron density models with many parameters, as we have shown by simulated examples. Indeed, in principle, the high q part of $F(q)$ could be obtained by analytic continuation of the low q portion. In practice, there is experimental error that leads to uncertainty in extrapolation from low q to high q, so one can not expect to separate structural features, such as two Gaussians in the headgroup region, that are much closer together than D/h_{max}. Nevertheless, it would appear that the model approach might still improve upon Fourier reconstructions and should certainly be employed as a supplement.

The preceding argument in favor of electron density models hinges substantially upon how well the true electron density is represented by the particular model functional form chosen. We have tested the hybrid models by fitting them to two molecular dynamics simulations of electron density for DPPC (Tu et al., 1995; Feller et al., 1995) and one for dimyristoylphosphatidylcholine (DMPC) (Chiu et al., 1995), as shown in Fig. 7. The 1G hybrid model provides quite a good representation of all three sets of simulation data. Because of asymmetry, employing two Gaussians (2G model) in the headgroup region does improve the fit (not shown) to the results of Tu et al. (1995) and the headgroup peaks of the results of Feller et al. (1995)

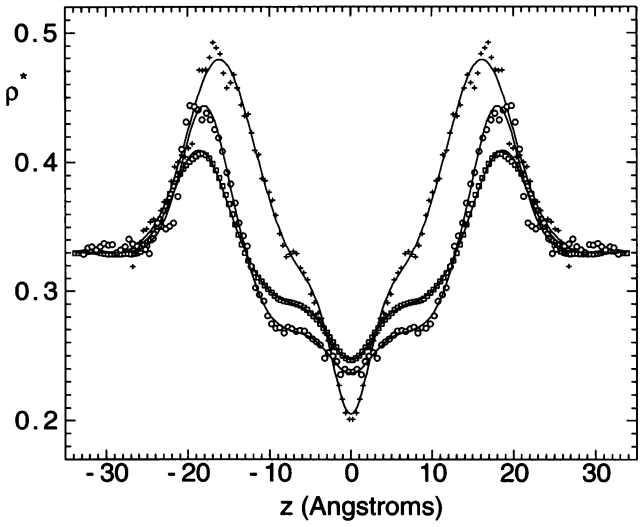

FIGURE 7 Symbols are symmetrized electron densities from three molecular dynamics simulations: open squares, Tu et al. (1995); open circles, Feller et al. (1995); +, Chiu et al. (1995). The solid lines show the best fitted hybrid electron density models with one Gaussian in the headgroup region.

are decidedly not symmetric, though with the opposite asymmetry as the headgroup peaks of Tu et al. (1995). The hybrid models were designed with the assumption 1) that each methylene volume V_{CH_2} is nearly constant whether it is near the center of the bilayer or nearer the headgroups (Nagle and Wiener, 1989). It has also been assumed (Nagle and Wiener, 1988) from liquid alkane studies 2) that the terminal methyls on the hydrocarbon chains have about twice the volumes of the methylenes, $V_{CH_3} = 2V_{CH_2}$. If assumptions (1) and (2) are true, then the effective hydrocarbon number density, defined as $n_{CH_2} + 2n_{CH_3}$, should be constant as a function of z along the bilayer normal in the central hydrocarbon region that is seldom penetrated by other groups. The results of the simulations shown in Fig. 8 basically support these assumptions, especially the simulations of Tu et al. (1995), which give quite constant effective hydrocarbon numbers in the hydrocarbon region.

In addition to having to obey Eq. 4, which we will call the $F(0)$ constraint, there is a second general relation for the hybrid models (Nagle and Wiener, 1989) that relates A to the size, S_M, of the methyl trough in the electron density profile,

$$A = 2[V_{CH_3}\rho^*_{CH_2} - n^*_{CH_3}]/S_M, \qquad (8)$$

where $n^*_{CH_3} = 9$ is the number of electrons in methyl groups. In principle, this would be another way to determine A in addition to Eq. 7. Unfortunately, our experience with fitting both real and simulated data indicates that the errors in the values of S_M determined from unconstrained fits are too large for this method to provide precise results for A. Instead, Eq. 8 has been used to constrain the size S_M of the methyl trough using a value of $A = 62$ Å^2, this will be called the methyl trough constraint. A third constraint, which will

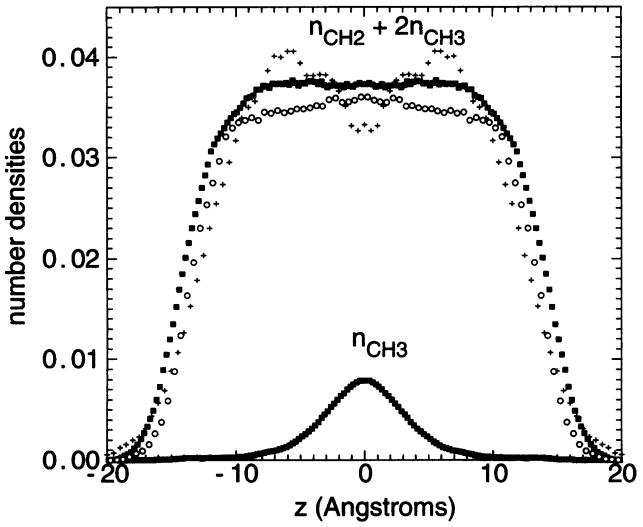

FIGURE 8 Effective hydrocarbon number densities $n_{CH_2} + 2n_{CH_3}$ in units of $Å^{-3}$. Solid squares from Tu et al. (1995); open circles from Feller et al. (1995); + from Chiu et al. (1995). Methyl number density is shown only for results from Tu et al.

be called the methylene constraint, was used extensively in modeling the gel phase (Wiener et al., 1989). This constrains the value of the methylene electron density $\rho^*_{CH_2}$. From volume measurements (Nagle and Wilkinson, 1978; Nagle and Wiener, 1988), $V^F_{CH_2}$ has been estimated to be 27.6 $Å^3$, which yields $\rho^*_{CH_2} = 0.290$ electrons/$Å^3$.

Our results are shown in Fig. 9 for 1G electron density models. We also attempted to fit 2G models, but there were many local minima found in the fitting that corresponded to

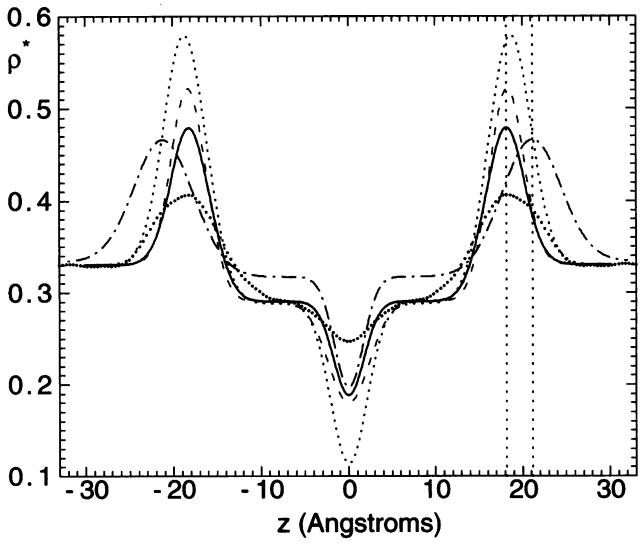

FIGURE 9 Several results for 1G models of the absolute electron density $\rho^*(z)$ as a function of distance z along the normal to the bilayer with the center of the bilayer at $z = 0$. *Dot-dash line*: gel phase. *Dotted line*: methylene constraint only. *Dashed line*: $F(0)$ and methylene constraints. *Solid line*: $F(0)$, methylene and methyl trough constraints. *Small solid circles*: simulation results from Tu et al. (1995). The vertical dotted lines indicate the difference in half X_{HH} between the gel and the fluid phases.

different proportions of the two head group Gaussians and their locations; this confirms that the data did not extend to high enough direct spatial resolution (not to be confused with our high instrumental resolution in reciprocal space) to distinguish fine features of the headgroup region. Because it is desirable to compare with gel phase electron densities at the same spatial resolution, the 1G gel phase result with $X_{HH} = 42.4$ Å (Wiener et al., 1989) is shown in Fig. 9.

When none of the three constraints described above are used, the hybrid model cannot be put on an absolute scale. This totally unconstrained fit can be easily normalized by using the methylene constraint and this is shown in Fig. 9 by the dotted curve. However, the size of the methyl trough is so large that Eq. 8 gives the absurd value, $A^F = 31$ $Å^2$. Another way to scale this unconstrained fit is to impose the methyl trough constraint instead of the methylene constraint; using $A^F = 62$ $Å^2$ reduces the sizes of the headgroup peaks and the methyl trough by a factor of two and the ensuing curve (not shown) is in better conformity with the other curves in Fig. 9, except that the electron density in the methylene region increases to $0.31e/Å^3$. Also, with either of these constraints, $F(0)$ is strongly positive and the ratio of $F(0)$ to $F(1)$ is of order -0.25 rather than close to zero as required by volumetric data. Therefore, it is necessary to consider fits with additional constraints. (It is worth noting, however, that $X_{HH} = 37.4$ Å for the dashed line; by Eq. 7 this gives $A^F = 62.0$ $Å^2$.)

Because the $F(0)$ constraint appears to be experimentally required, all our additional results use it. Unfortunately, because $F(0)$ is effectively zero, this constraint does not allow the electron densities to be put on an absolute scale. Therefore, our next model, shown by the dashed line in Fig. 9, also adds the methylene constraint. This model predicts, by Eq. 8, that $A^F = 42.8$ $Å^2$, which is still smaller than A^G and the headgroup peaks are rather large. We also tried using both the $F(0)$ and the methyl trough constraint but not the methylene constraint (electron density profile not shown on Fig. 9), and this resulted in a best value of $\rho^*_{CH_2} = 0.308e/Å^3$, which seems too high. We therefore finally fit the form factor data with all three constraints. We used a trial value of $A^F = 62$ $Å^2$ in the methyl trough constraint, but all subsequent results, especially the result for headgroup position X_{HH} and the ensuing value of A^F obtained from Eq. 7, are insensitive to 10% variations in this trial value. We also favored fits that gave broader electron density features and smaller $F(q)$ values for large q by adding zero values with noise levels comparable to the data for 11 random q values greater than 0.6 $Å^{-1}$. The resulting electron density profile is shown by the solid curve in Fig. 9, and the continuous transform $F(q)$ and the fit of the measured form factors are shown in Fig. 10. The scaled values of $F(1)$ that appear in Table 1 correspond to Fig. 10. The electron density profile shown by the solid curve in Fig. 9 gives $X_{HH} = 36.4$ Å which, by Eq. 7, gives $A^F = 64.2$ $Å^2$. Although this latter value of A^F is different from the trial value of A^F used in the methyl trough constraint, this makes very little difference in the value of X_{HH} obtained from the fits.

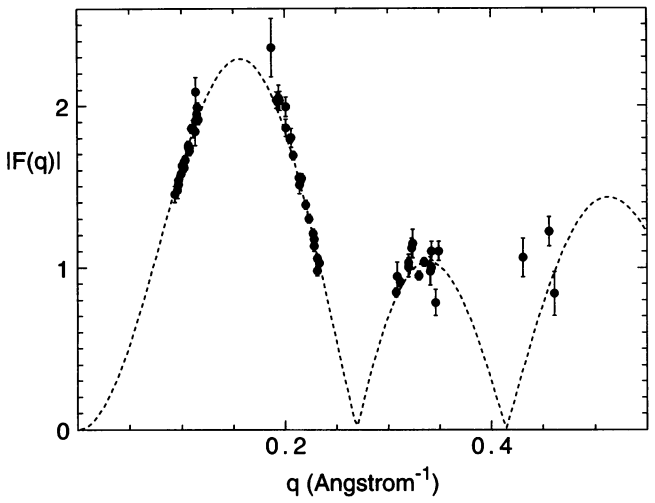

FIGURE 10 Best fit of 1G model to our data, with the methylene constraint, methyl trough constraint, and the $F(0) = 0$ constraint. The dashed line is the fit, and the solid circles are the form factor data for q less than 0.6 Å^{-1}.

A^F from neutron diffraction studies

Our main result that bilayer structure does not change with mild dehydration down to $D = 54$ Å suggests that the older neutron diffraction results (Buldt et al., 1979) that were obtained for $D = 54.1$ Å, should be valid for fully hydrated L_α phase DPPC. We here show two ways that those results can be used to obtain A^F. The first way to use the neutron results employs Eq. 7, but instead of using electron densities to obtain $(X^G_{HH} - X^F_{HH})/2$, the differences in the locations of various molecular groups between the fully hydrated gel and L_α phases are used. The headgroup labels at the C_α, C_β, and C_γ positions yield $(X^G_{HH} - X^F_{HH})/2 = 2.6$, 2.9, and 2.6 Å, respectively. The hydrocarbon chain labelled at the C_4 position yields $(X^G_{HH} - X^F_{HH})/2 = 3.1$ Å. Only the glycerol label GC3 is out of line with $(X^G_{HH} - X^F_{HH})/2 = 4.2$ Å. Discounting this latter result and averaging the other values gives $(X^G_{HH} - X^F_{HH})/2 = 2.8$ Å and a value $A^F = 63.3$ Å^2 using Eq. 7. The second way uses the results for the positions of the fourth and fifth methylenes, $z^{(4)}_{CH_2} = 12.2$ Å and $z^{(5)}_{CH_2} = 10.5$ Å (although it may be noted that these two spacings are mutually inconsistent because their difference exceeds the C–C bond length of 1.54 Å). We take the average spacing of 11.4 Å to include, on average, all the methylenes with carbon number 5 or greater and all the terminal methyls. Assuming that the volume of each terminal methyl is twice the volume of each methylene, one has

$$A^F = 26\, V_{CH_2}/(11.4\text{ Å}) = 62.9\text{ Å}^2, \quad (9)$$

where $V_{CH_2} = 27.6$ Å^3 (Nagle and Wiener, 1988).

A^F and other quantities

For our final estimate of A^F from diffraction studies, we first average our two x-ray results, 61.2 Å^2 from Fourier analysis and 64.2 Å^2 from hybrid modeling, with the two results, 63.3 Å^2 and 62.9 Å^2, obtained from neutron diffraction results in the preceding paragraph. This gives our final diffraction estimate, $A^F = 62.9 \pm 1.3$ Å^2.

Once the area A^F is determined, a number of other quantities follow from simple relations described by Nagle and Wiener (1988). One of the most illuminating quantities is the number of water molecules n_w per lipid molecule between the bilayers in regular multilamellar vesicles; this is easily calculated from

$$n_w = [(AD/2) - V_L]/V_w \quad (10)$$

where $V^F_L = 1232$ Å^3 and $V_W = 30.3$ Å^3 at 50°C in the L_α phase and $V^G_L = 1144$ Å^3 and $V_W = 29.9$ Å^3 at 20°C in the gel phase. In addition to representing the bilayer thickness as X_{HH}, it is also frequently represented as D_B, which is the volume fraction of the D spacing that would be occupied by the lipid bilayer if the interface with water were a plane. D_B is given by

$$D_B = 2V_L/A. \quad (11)$$

and the corresponding water spacing is then $D_w = D - D_B$. Of course, the bilayer/water interface is not so simple, so a slightly more complex model (Nagle and Wiener, 1988) assumes that the headgroup (which includes the acyl chain carbonyls) has a length D'_H over which it has a uniform area A'. This model then allows for penetration of n'_w waters in the volume D'_H $(A - A')$ between the headgroups. From neutron diffraction (Buldt et al., 1979), $D'_H = 8$ Å appears to be a generously large estimate. Then, a corresponding pure water distance $D'_w = D - 2D'_H - 2D^F_C$ is defined where the total hydrocarbon thickness is defined by $2D^F_C$ and is calculated using Eq. 6. A summary of the values of these derived quantities as well as measured quantities is given in Table 2 for the L_α phase for two values of D near the extremes of our data as well as earlier results (Sun et al., 1994) for the fully hydrated gel phase.

DISCUSSION

Our primary experimental results are the ratios of form factors f_h reported in Table 1 for various levels of hydration. These

TABLE 2 Structural quantities for L_α and $L_{\beta'}$ phase dipalmitoylphosphatidylcholine bilayers

Quantity	L_α (50°C)		$L_{\beta'}$ (20°C)
D (Å)	67.2	53.9	63.4
$X^{h=4}_{HH}$ (Å)	—	39.6	44.2
X^{1G}_{HH} (Å)	36.4	36.4	42.4
A (Å^2)	62.9	62.9	47.9
D_B (Å)	39.2	39.2	47.8
D_W (Å)	28.0	14.7	15.6
n_W	29.1	15.3	12.6
D_c (Å)	14.6	14.6	17.2
D'_W (Å)	22.0	8.7	13.0
n'_W	6.3	6.3	2.2

data provide a basic test for theoretical models of L_α phase DPPC bilayers, such as those obtained from computer simulations, much like the traditional S_{CD} NMR order parameters (Seelig, 1977) that are most frequently employed as a test. To perform this test electron density profiles obtained by theory should be Fourier transformed to obtain f_h.

The particular innovation used in this study to obtain the f_h is the combined use of x-ray scattering at very high instrumental resolution and the modified Caillé peak shape theory (Zhang et al., 1994) to obtain the true scattering intensity under the entire peak, including the long power law tails predicted by this theory and verified experimentally (Roux and Safinya, 1988; Zhang et al., 1996). This analysis obtains the Caillé η_1 fluctuation parameter, which is shown in Fig. 2 and which decreases as D spacing decreases. From the definition of η_1 following Eq. 1, this suggests that the compression modulus B increases with dehydration and that the interactions between bilayers become stronger as the water space decreases. Further analysis of the forces involved will be deferred to another paper. Most importantly for this paper, this analysis of the experimental data is essential to obtain the correct continuous scattering transform $F(q)$ and to explain why some of the higher order peaks for the more hydrated samples cannot be seen.

Our $F(q)$ transform in Fig. 4 is consistent with no change in bilayer structure for the L_α phase of DPPC as the bilayer is dehydrated from a D spacing of 67.2 Å to 53.9 Å. As is shown by Fig. 5, this conclusion cannot be drawn if one performs a straightforward integration of the central peak intensities that ignores the long power law tails. Even the form factors for the $h = 2$ order are systematically too small with higher hydration, and some of the $h = 3$ orders should have been seen, but could not be. However, we now know that this is due to the loss of intensity into the tails, which is impossible to separate from background without an appropriate theory to perform the extrapolation from the measured peak shapes. This in turn requires high resolution x-ray detection that was achieved with our experimental configuration at CHESS.

We conclude from our data that the threshold spacing D_T, above which the bilayer structure effectively does not change, must be smaller than 54 Å. This conclusion is supported by the results of Torbet and Wilkins (1976) for the gel phase of DPPC which showed that fairly small changes in bilayer thickness resulted in rather large changes in the continuous transform. This conclusion disagrees with conclusions drawn from x-ray studies using the gravimetric method of Luzzati, which indicated that bilayer structure changed continuously as the system is dehydrated from full hydration (Tardieu et al., 1973; Lis et al., 1982). The latter conclusion had implied that results from studies on partially dehydrated samples, such as the classic neutron diffraction studies on specifically deuterated lipids (Buldt et al., 1979; Zaccai et al., 1979) where the D-spacing was 54.1 Å, are biologically less relevant. One likely source of error in the gravimetric method is the assumption that all the water resides neatly between the bilayers (Wiener et al., 1989; Klose et al., 1988). This is quite unlikely for multilamellar vesicles (MLV) that must have extra water in small volumes in the center of each MLV as well as in regions between different MLVs. Only in well-oriented planar arrays could one hope that this assumption is valid. Also, the areas A from gravimetric studies have been consistently larger than those obtained by other methods; this discrepancy is also explained by the assumption about water residence being incorrect. In the case of gel phase DPPC, we have shown previously for both oriented- (Tristram-Nagle et al., 1993) and powder-multilamellar vesicular samples (Sun et al., 1994) that the gravimetric method gave erroneously large results for A. Although our present results do not go to low enough hydration to find the value of the dehydration threshold D_T, they do require that D_T be smaller than 54 Å and this suffices to validate the biological relevance of the neutron diffraction results for L_α phase DPPC at 50°C as well as to provide support for x-ray studies that attempt to obtain membrane structure for partially dehydrated samples.

On the other hand, because one would expect that dehydration would alter the forces between bilayers and that this could change their structure, it is worth discussing quantitatively how much dehydration was required to obtain samples with $D = 54$ Å. In Table 2 it is shown that only a little less than half the water must be removed, leaving $n_w = 15.5$ waters even when $D = 54$ Å. This is even more water than resides in the fully hydrated gel phase. Also, the mean pure water spacing $D_W' = 9$ Å between headgroups is still large enough to avoid much direct contact between headgroups on adjacent bilayers because, as shown by Zhang et al. (1996), the mean fluctuation in adjacent bilayer spacing is only about ±3 Å for the value of $\eta_1 = 0.03$ that is obtained for $D = 54$ Å from Fig. 2. Furthermore, the relative humidity for our most dehydrated samples is still about 98%. In addition, we have performed differential scanning calorimetry on this sample and find that the main transition temperature T_M rises at most 0.7°C; this is much less than the rise in T_M for fully dehydrated samples, which exceeds 20°C. Finally, the work W done against the hydration force is given by the product of the osmotic pressure of our most dehydrated sample ($P_{osm} = 24$ atm), the area A^F, and the decay length λ, which is given as 1.7 Å for egg lecithin (McIntosh and Simon, 1986a); this yields 0.03 kcal/mol, which is considerably less than the enthalpy 8.7 kcal/mol for the main phase transition, which sets the scale for major structural changes. Therefore, our experimental result that bilayer structure does not change measurably upon dehydrating to $D = 54$ Å is theoretically plausible and consistent with our determination of structure reported in Table 2.

It may also be noted that the threshold hypothesis implies that there is unlikely to be any structural difference between bilayers in large unilamellar vesicles and those in multilamellar vesicles. This follows because the interbilayer interactions become considerably stronger upon dehydration. If these increasingly stronger interactions do not change the bilayer structure, then the weaker interbilayer forces present in fully hydrated multilamellar vesicles would not change

the bilayer structure compared to isolated large unilamellar vesicles.

Electron density profiles have been obtained in two ways. The first and most straightforward way that has been employed by many previous workers is to plot the Fourier series using the maximum number of orders of diffraction, which for our data is $h_{max} = 4$. Earlier use of this procedure has also indicated that the thickness of bilayers does not change upon dehydrating with PVP for either the gel phase of DPPC or the L_α phase of egg lecithin (McIntosh, 1986a). One of our concerns with this earlier conclusion was that fluctuation corrections were not made and that this would be expected to distort the form factors as shown in Fig. 5 compared with Fig. 4. However, our result in Fig. 6 and our theory in the Appendix shows that fluctuation corrections have almost no effect upon the apparent head-head spacing X_{HH} and this was the major result required by the earlier work. Because only the widths of the peaks and the methyl troughs are affected, our results therefore support the methodology of the earlier work as well as the conclusion that there is little change in bilayer structure upon mild dehydration.

A major goal that we believe we have achieved is to obtain the area A^F for L_α phase DPPC at 50°C, which is the most commonly compared temperature. Although A^F does not depend upon hydration down to the D_T threshold, it is expected to depend fairly strongly on temperature, especially near the main transition T_M (Zhang et al., 1995), as well as exhibiting a gradual increase with increasing T above 50°C, but we have not included these effects in this study. Our primary method was adapted from one introduced by McIntosh and Simon (1986b) that obtains A^F for the L_α phase from Eq. 7, which uses gel phase quantities (Tristram-Nagle et al., 1993; Sun et al., 1994), measured volume changes (Nagle and Wiener, 1988), and the changes in the head-head positions, $(X^G_{HH} - X^F_{HH})/2$, that are obtained in this paper. The Fourier method works quite well, yielding $(X^G_{HH} - X^F_{HH})/2 = 2.3$ Å and $A^F = 61.2$ Å, despite having only three samples with $h_{max} = 4$ orders.

We have also used a method of analysis that treats all the data with different D spacings globally. This method requires a model electron density function. We have used the hybrid model proposed earlier (Nagle and Wiener, 1989) after showing in Fig. 7 that it adequately represents the electron density profiles of current molecular dynamics simulations, which also agree with the main assumption that the methylene density is effectively constant in the hydrocarbon region as shown in Fig. 8. There are three constraints on the electron density profile (Nagle and Wiener, 1989) that have been employed to yield the various experimental electron density profiles as shown in Fig. 9. Our methodology for calculating area using Eq. 8 then yields $A^F = 64.2$ Å^2.

The values of X_{HH} in the experimental electron density profiles in Fig. 9 are in excellent agreement with the recent simulation of Tu et al. (1995), also shown in Fig. 9, which has $X_{HH} = 36.4$ Å. One discrepancy that arises is that use of this value X_{HH} in Eq. 7 yields $A^F = 64.2$ Å^2 which is larger than $A^F = 61.8$ Å^2 obtained from the simulation. However, the same spatial resolution and methodology should be used for both the gel and the fluid phases in calculating the difference in X_{HH}, so we should use the value $X_{HH} = 37.2$ Å^2 obtained from a 1G fit to the simulated electron density profile (see Fig. 7). This yields $A^F = 62.4$ Å^2 from Eq. 7, which is satisfactorily close to 61.8 Å^2 and supports our methodology for obtaining A^F. Another minor inconsistency arises from applying Eq. 8 to our 1G fit to the simulated methyl trough of Tu et al. (1995). This yields $A^F = 101$ Å^2 assuming that $V_{CH_3}/V_{CH_2} = 2$ and that $\rho^*_{CH_2} = 0.29e$/Å^3; the latter value appears consistent with the simulated curve in Fig. 9 and also emerges from our 1G fit to these data. However, the plateau level for the number density in Fig. 8 gives $\rho^*_{CH_2}$ closer to $0.30e$/Å^3. Using this latter value of $\rho^*_{CH_2}$ changes the size of the methyl trough so that A^F then yields 62 Å^2 using Eq. 8. While this removes the inconsistency, it warns one that, despite the good fit of the 1G model to the simulated data, the parameters for $\rho^*_{CH_2}$ that emerge from the fit seem to be corrupted by mixing with other parameters so that Eq. 8 does not give accurate values for A^F. Another discrepancy is that our hybrid model headgroup peaks are much higher than the simulated headgroup peaks in Fig. 9. In this latter regard, our best hybrid model result shown by the solid line in Fig. 9 agrees better with the simulations of Feller et al. (1995) shown in Fig. 7, even though these simulations were performed at a larger constant area of $A^F = 68.1$ Å^2 and consequently have a smaller $X_{HH} = 36.0$ Å^2 when fitted to a 1G model.

The most surprising result in Fig. 9 is the relative narrowness of our headgroup peaks and the methyl trough. The 1G methyl trough for our fully constrained fit has a half-width ($\sigma^F_{CH_3} = 1.77$ Å), not much wider than the 1G methyl trough for the gel phase ($\sigma^G_{CH_3} = 1.67$ Å) and narrower than the Gaussian fit to the simulation methyl trough ($\sigma^S_{CH_3} = 2.61$ Å). The 1G headgroups have half-widths ($\sigma^F_H = 2.25$ Å) that are narrower than the gel phase results ($\sigma^G_H = 3.43$ Å) and the fluid phase simulations ($\sigma^S_H = 3.5$ Å). It is possible that the narrowness of our model electron density profiles is related to intrinsic errors in analytically continuing the $F(q)$ curve to high q. Although the lack of data at higher angles always broadens features in Fourier reconstructions of the electron density profile, this is not necessarily the case for the model method, as we have confirmed by taking a known model electron density profile, Fourier analyzing it, adding noise to the Fouriers, fitting models to the Fouriers, and then comparing to the original model electron density. Finally, when we did a fit with all three constraints, but with $\rho^*_{CH_2}$ fixed to $0.304e$/Å^3, the methyl trough half-width increased substantially to $\sigma^F_{CH_3} = 2.5$ Å. In contrast, $X_{HH}/2$ only increased by 0.1 Å, so widths of features in the hybrid model may be less certain than the head-head spacing, which is the crucial quantity for obtaining the area A^F.

Our main result that bilayer structure does not change with mild dehydration down to 54 Å allows us to use the older neutron diffraction results, which were obtained for $D = 54.1$ Å, in two new ways to obtain additional estimates,

63.3 Å^2 and 62.9 Å^2, for A^F. For our final estimate of A^F, we averaged these with two x-ray results, 61.2 Å^2 from Fourier analysis and 64.2 Å^2 from hybrid modeling, to obtain our final diffraction result, $A^F = 62.9 \pm 1.3$ Å^2 in the L_α phase of DPPC at 50°C.

The other major way of determining A^F uses the S_{CD} NMR order parameters. Although the NMR method has been employed in several different ways giving considerably different values of A^F, our recent analysis gave $A^F = 62 \pm 2$ Å^2 for DPPC under the same conditions as in this paper (Nagle, 1993), in good agreement with the present diffraction result. Even the sign of the small difference can be understood because the NMR result assumed no backtracking of chains, which, if present, would increase the NMR estimate of A^F. As more quantitative information about backtracking becomes available from simulations, quantitative changes in the NMR estimate can be made.

Our value of A^F is smaller than the value $A^F = 66.5$ Å^2 determined for unilamellar vesicles by Lewis and Engelman (1983) using weak continuous scattering. It is considerably smaller than the $A^F = 71$ Å^2 obtained by the gravimetric method (Lis et al., 1982) or the $A^F = 68.1$ Å^2 obtained by modifying that method (Rand and Parsegian, 1989) to try to account for inconsistency with lateral compressibility data. This latter value of A^F was assumed in the simulations of Feller et al. (1995). A recent simulation (Essmann et al., 1995) used a fixed value $A^F = 65.8$ Å^2 for nearly fully hydrated DPPC with $n_w = 20.5$. Other recent simulations employ constant pressure ensembles rather than constant area ensembles and this allows for the simulation to determine the best A^F. Chiu et al. (1995) obtain the smaller $A^F = 57.3$ Å^2 at 52°C, but this was for DMPC. The recent simulations for DPPC by Tu et al. (1995) yield $A^F = 61.8$ Å^2, in excellent agreement with our values for A^F.

The variety of simulation results for ostensibly the same lipid bilayer emphasizes that there are many noncanonical choices to be made when doing a simulation. It is clearly important that critical experimental data be available to test choices in potentials, effect of initial configuration (because effective running times are only ns, during which the system may hang in a metastable state), and choice of ensemble parameters such as effective lateral pressure. In this regard, we emphasize that the ratios of form factors in Table 1 should be compared to simulations. (Direct comparison to our primary data, the scattering peaks, would require simulations on bilayers of square micron size, which is unlikely to be feasible). However, we emphasize that simulation results, even if all the simulation choices are not perfect and even if all the simulations do not agree, are extremely valuable in testing assumptions used in analyzing data, as we show in Figs. 7 and 8 in this paper and as was previously mentioned in the analysis of NMR data (Nagle, 1993).

Fluid L_α phase lipid bilayers are difficult to study experimentally, because of their partially ordered/disordered nature that gives rise to nontrivial fluctuations. We believe the present study has made substantial progress on this point. We anticipate that combined experimental and simulation studies will resolve remaining issues and provide a methodological foundation for quantitatively comparing bilayers composed of different lipids.

APPENDIX

The modified Caillé theory (Zhang et al., 1994; Zhang, 1995) shows that the effect of fluctuations reduces the apparent form factors $F_a(h)$ compared to the true form factors $F(h)$ according to the approximate formula

$$F_a(h) = C^{1/2} F(h) W^{-h^2}, \tag{A1}$$

where C is nearly constant as a function of order h,

$$W = \left(\frac{\Delta q}{1.78 q_1}\right)^{\eta_1/2}, \tag{A2}$$

and $2\Delta q$ is the interval over which the data are integrated to obtain the apparent, uncorrected intensity of the peak. If $\eta_1 \ll 1$, i.e., there are several observable peaks, the apparent electron density $\rho_a(z)$, obtained from the apparent form factors F_a in Eq. A1, are related to the true electron density $\rho(z)$ by the following convolution integral

$$\rho_a(z) = \rho(z) * U(z), \tag{A3}$$

where

$$U(z) = \frac{C^{1/2}}{D}\left[\frac{\pi}{\ln W}\right]^{1/2} e^{-(\pi z/D)^2/\ln W}. \tag{A4}$$

We call $U(z)$ the smearing function; it is essentially a Gaussian whose half-width at half maximum,

$$HW_U = \frac{D}{\pi}\left(\frac{\eta_1}{2}\right)^{1/2} [(0.577 + \ln(q_1/\Delta q))\ln 2]^{1/2}, \tag{A5}$$

depends strongly on η_1. Fig. 11 shows how a typical $U(z)$ smearing function broadens the electron density features of a hybrid model. However, the apparent head to head distance $H_{H\text{-}H}$ is basically unchanged from the true distance; this latter result can be understood theoretically because

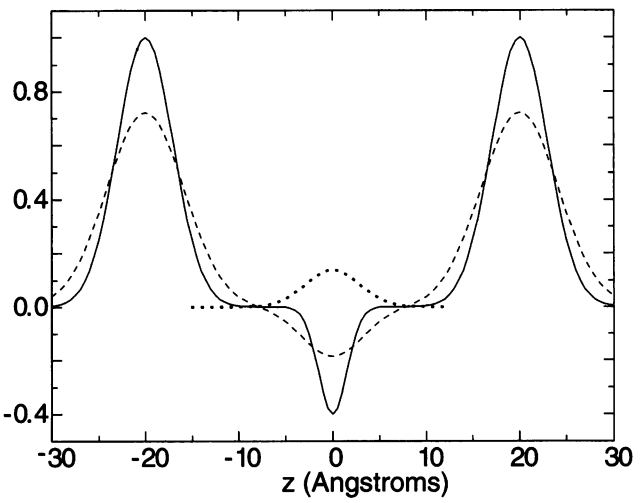

FIGURE 11 Smearing effect on electron density due to fluctuations. The solid line shows an unsmeared profile that is convoluted with the smearing function shown by the dotted line to produce the smeared electron density profile shown by the dashed line. The calculation of the smearing function used $\eta_1 = 0.03$ and $\Delta q/q_1 = 0.1$.

the convolution of a Gaussian smearing function with a symmetric headgroup peak leaves the center of the resulting peak position unchanged.

Traditionally, the smearing effect shown in Fig. 11 was treated by assuming that the true form factor was multiplied by an ad hoc Debye-Waller type of temperature factor (Franks and Lieb, 1979; Torbet and Wilkins, 1976; Zaccai et al., 1975)

$$F_a(h) = F(h)e^{-B_{DW}h^2/4D^2}. \quad \text{(A6)}$$

The B_{DW} factor for a rather dry bilayer system was taken to be zero; and B_{DW} for a higher water content bilayer system was then determined by matching the $\rho(z)$ for that high water content bilayer system with the $\rho(z)$ calculated using $F_a(h)$ in Eq. A6 and $I_{int}(h)$ data from the very low water content bilayer system, assuming that the bilayer structure does not change within that hydration range. Eq. A6 has a very similar form to Eq. A1. However, in contrast to the use of Eq. A6, in our use of Eq. A1 the parameter η_l is determined by fitting the peak shapes. Therefore, our theory does not require the assumption that the bilayer shape is unchanged, and therefore allows us to test it. Although one could devise a similar procedure based upon Eq. A6, this requires an additional unknown Debye-Waller parameter B_{DW} for each data set from samples with different water content. Therefore, whereas our method justifies the form of the older method, it also improves upon it.

For providing the results of molecular dynamics simulations shown in Figs. 7 and 8, we thank the members of three simulation groups, particularly Scott Feller, Richard Venable, and Richard Pastor; Larry Scott; Michael Klein, Doug Tobias and especially Kechuan Tu for visits to our laboratory and extensive interaction. We thank our CHESS collaborators R. L. Headrick and T. C. Irving for their help in acquiring the basic scattering data. Synchrotron beam time was provided under CHESS proposal P619. This research was supported by National Institutes of Health Grant No. GM44976.

REFERENCES

Buldt, G., H. U. Gally, J. Seelig, and G. Zaccai. 1979. Neutron diffraction studies on phosphatidylcholine model membranes I: head group conformation. *J. Mol. Biol.* 134:673–691.

Caillé, A. 1972. Physique cristalline - Remarques sur la diffusion des rayons X dans les smectiques *A. C. R. Acad. Sc. Paris,* Série B 274: 891–893.

Chiu, S.-W., M. Clark, V. Balaji, S. Subramanian, H. L. Scott, and E. Jakobsson. 1995. Incorporation of surface tension into molecular dynamics simulations of an interface: a fluid phase lipid bilayer membrane. *Biophys. J.* 69:1230–1245.

DeGennes, P. G. 1974. The Physics of Liquid Crystals. Oxford Press, Clarendon. 284–286.

Essmann, U., L. Perera, and M. L. Berkowitz. 1995. Simulation of DPPC membranes in gel and liquid crystalline phases. *Langmuir.* 11: 4519–4531.

Feller, S. E., Y. Zhang, and R. W. Pastor. 1995. Computer simulation of liquid/liquid interfaces. II. Surface tension—area dependence of a bilayer and monolayer. *J. Chem. Phys.* 103:10267–10276.

Franks, N. P., and W. R. Lieb. 1979. The structure of lipid bilayers and the effects of general anaesthetics, an X-ray and neutron diffraction study. *J. Mol. Biol.* 133:469–500.

Klose, G., B. Konig, H. W. Meyer, G. Schulze, and G. Degovics. 1988. Small-angle x-ray scattering and electron miscroscopy of crude dispersions of swelling lipids and the influence of morphology on the repeat distance. *Chem. Phys. Lipids.* 47:225–234.

Lewis, B. A., and D. M. Engleman. 1983. Lipid bilayer thickness varies linearly with acyl chain length in fluid phosphatidylcholine vesicles. *J. Mol. Biol.* 166:211–217.

Lis, L. J., M. McAlister, N. Fuller, R. P. Rand, and V. A. Parsegian. 1982. Interactions between neutral phospholipid bilayer membranes. *Biophys. J.* 37:657–666.

McIntosh, T. J., and S. A. Simon. 1986a. Hydration and bilayer deformation: a reevaluation. *Biochemistry.* 25:4058–4066.

McIntosh, T. J., and S. A. Simon. 1986b. Area per molecule and distribution of water in fully hydrated dilauroylphosphatidylethanolamine bilayers. *Biochemistry.* 25:4948–4952.

Nagle, J. F. 1980. Theory of the main lipid bilayer phase transition. *Annu. Rev. Phys. Chem.* 31:157–195.

Nagle, J. F. 1993. Area/lipid of bilayers from NMR. *Biophys. J.* 64: 1476–1481.

Nagle, J. F., and M. C. Weiner, 1988. Structure of fully hydrated bilayer dispersions. *Biochim. Biophys. Acta.* 942:1–10.

Nagle, J. F., and M. C. Wiener, 1989. Relations for lipid bilayers: connection of electron density profiles to other structural quantities. *Biophys. J.* 64:1476–1481.

Nagle, J. F. and D. A. Wilkinson. 1978. Lecithin bilayers: density measurements and molecular interactions. *Biophys. J.* 23:159–175.

Rand, R. P., and V. A. Parsegian. 1989. Hydration forces between phospholipid bilayers. *Biochim. Biophys. Acta.* 988:351–376.

Roux, D., and C. R. Safinya. 1988. A synchrotron X-ray study of competing undulation and electrostatic interlayer interactions in fluid multimembrane lyotropic phases. *J. Phys. France.* 49:307–318.

Tardieu, A., V. Luzzati, and F. C. Reman. 1973. Structure and polymorphism of the hydrocarbon chains of lipids: a study of lecithin-water systems. *J. Mol. Biol.* 75:711–733.

Seelig, J. 1977. Deuterium magnetic resonance: theory and application to lipid membranes. *Quart. Rev. Biophys.* 10:353–418.

Sun, W.-J., R. M. Suter, M. A. Knewtson, C. R. Worthington, S. Tristram-Nagle, R. Zhang, and J. F. Nagle. 1994. Order and disorder in fully hydrated unoriented bilayers of gel phase DPPC. *Phys. Rev. E* 49: 4665–4676.

Torbet, J., and M. H. F. Wilkins. 1976. X-ray diffraction studies of lecithin bilayers. *J. Theor. Biol.* 62:447–458.

Tristram-Nagle, S., R. Zhang, R. M. Suter, C. R. Worthington, W.-J. Sun, and J. F. Nagle. 1993. Measurement of chain tilt angle in fully hydrated bilayers of gel phase lecithins. *Biophys. J.* 64:1097–1109.

Tu, K., D. J. Tobias, and M. L. Klein. 1995. Constant pressure and temperature molecular dynamics simulation of a fully hydrated liquid crystal phase dipalmitoylphosphatidylcholine bilayer. *Biophys. J.* 69: 2558–2562.

Wiener, M. C., S. Tristram-Nagle, D. A. Wilkinson, L. E. Campbell, and J. F. Nagle. 1988. Specific volumes of lipids in fully hydrated bilayer dispersions. *Biochim. Biophys. Acta.* 938:135–142.

Wiener, M. C., R. M. Suter, and J. F. Nagle. 1989. Structure of the fully hydrated gel phase of DPPC. *Biophys. J.* 55:315–325.

Wiener, M. C., and S. H. White. 1992. Structure of fluid DOPC determined by joint refinement of x-ray and neutron diffraction data III: complete structure. *Biophys. J.* 61:434–447.

Worthington, C. R. 1969. The interpretation of low-angle x-ray data from planar and concentric multilayered structures. *Biophys. J.* 9:222–234.

Worthington, C. R., G. I. King, and T. J. McIntosh. 1973. Direct structure determination of multilayered membrane-type systems which contain fluid layers. *Biophys. J.* 13:480–494.

Zaccai, G., J. K. Blasie, and B. P. Schoenborn. 1975. Neutron diffraction studies on the location of water in lecithin bilayer model membranes. *Proc. Nat. Acad. Sci. USA.* 72:376–380.

Zaccai, G., G. Buldt, A. Seelig, and J. Seelig. 1979. Neutron diffraction studies on phosphatidylcholine model membranes. *J. Mol. Biol.* 134: 693–706.

Zhang, R. 1995. Lecithin bilayers in fluid phase: effect of fluctuations on x-ray determination of structure. Ph. D. thesis. Carnegie Mellon University.

Zhang, R., R. M. Suter, and J. F. Nagle. 1994. Theory of the structure factor of lipid bilayers. *Phys. Rev. E.* 50:5047–5060.

Zhang, R., W. Sun, S. Tristram-Nagle, R. L. Headrick, R. M. Suter, and J. F. Nagle. 1995. Critical Fluctuations in Membranes. *Phys. Rev. Lett.* 74:2832–2835.

Zhang, R., W. Sun, S. Tristram-Nagle, R. L. Headrick, T. C. Irving, R. M. Suter, and J. F. Nagle. 1996. Small angle x-ray scattering from lipid bilayers is well described by modified Caillé theory, but not by paracrystalline theory. *Biophys. J.* 70:349–357.